Urban Climate 56 (2024) 102042

Contents lists available at ScienceDirect

Urban Climate

journal homepage: www.elsevier.com/locate/uclim

Pavement watering as an urban heat mitigation technique

Ellie Traill [b,c], Kerry A. Nice [a,*], Nigel Tapper [b], Julie M. Arblaster [b,c]

[a] Transport, Health, and Urban Systems Research Lab, Faculty of Architecture, Building and Planning, University of Melbourne, VIC, Australia
[b] School of Earth, Atmosphere and Environment, Monash University, Clayton, VIC 3800, Australia
[c] ARC Centre of Excellence for Climate Extremes, Monash University, Melbourne, VIC, Australia

ARTICLE INFO

Keywords:
Urban climate
Urban heat island
Heat mitigation
Pavement watering
Thermal comfort

ABSTRACT

Climate change, rapid urbanisation, and ageing populations are reinforcing the need for urban heat mitigation techniques. Pavement watering is one such technique, where evaporative cooling is induced through wetting urban surfaces. The aim of this research is to assess the potential cooling benefits of pavement watering. To do this, a 10 × 10 m section of a car park was watered, and experiments were conducted at midday, the afternoon, and the evening across three days. Pavement watering was found to induce a mean cooling of up to 0.6 °C in air temperature and 2 °C in UTCI at 1.5 m. Benefits were related to prevailing conditions, with lower wind speeds associated with greater cooling. Surface temperature was also found to decrease by up to 9.0 °C, and the surface energy balance of the watered carpark was characteristic of a highly evaporative surface. However, there were limitations of the experiments; notably, the assumptions made to correct observations increased uncertainty, and the small scale of the experiment likely limited the observed cooling benefits. Despite this, pavement watering was shown to reduce air temperature and surface temperature, as well as improve thermal comfort, and thus may potentially be used in emergencies to provide cooling in urban areas.

1. Introduction

Urban areas are especially vulnerable to heat facing future trends of increased heatwave frequency and duration (Cowan et al., 2014; Perkins-Kirkpatrick and Lewis, 2020) driven by climate change (IPCC, 2022). In many urban areas in the world extreme heat is the most dangerous natural hazard, including Australia (Coates et al., 2014) and Europe (Forzieri et al., 2017), driving higher heat-related morbidity and mortality (Heidari et al., 2020) with disproportionate risks falling on vulnerable populations such as the elderly and the very young (Nicholls et al., 2008; Wilson, 2011). This risk further increases with ageing populations who are increasingly living in urban areas (ABS, 2013). The design of cities has exacerbated the risks associated with heat extremes, especially the process of replacing natural pervious land covers with hard heat-absorbent surfaces (Brunner and Cozens, 2013). This conversion combined with the reduction of available water in cities (Spronken-Smith and Oke, 2010; Coutts et al., 2012; Middel and Krayenhoff, 2019; Cheung et al., 2022), shifts the urban energy balance (Oke, 1982, 1989) away from latent heat (Q_E) towards increased sensible heat (Q_H) and increased heat storage (Q_S) in urban surfaces, resulting in higher canopy air and surface temperatures (Coutts et al., 2012; Martilli et al., 2020; Nice et al., 2022), and heat stress risks (Nicholls et al., 2008; Loughnan et al., 2010; Nazarian et al., 2022).

Thus, urban heat mitigation techniques are necessary. Strategies to mitigate urban heat can involve methods such as surface albedo changes, vegetation cover, irrigation, and the use of water (Krayenhoff et al., 2021). The use of water, specifically through evaporative

* Corresponding author.
E-mail address: kerry.nice@unimelb.edu.au (K.A. Nice).

https://doi.org/10.1016/j.uclim.2024.102042
Received 13 November 2023; Received in revised form 16 June 2024; Accepted 22 June 2024
Available online 5 July 2024

cooling induced through wetting urban surfaces, i.e. pavement watering, has been investigated as an emergency urban cooling technique. In Japan, pavement watering is tied to a 17th century Japanese custom, uchimizu, where water is sprinkled on streets outside houses and shops. Due to the cooling benefits, the practice is currently encouraged by Japanese authorities (Solcerova et al., 2018) and numerous field experiments on its effectiveness have been performed in Kinouchi (1997), Himeno et al. (2010), and Takebayashi et al. (2021, 2022, 2023). Pavement watering has also been utilised in Korea (Kim et al., 2014, 2015; Na et al., 2021) and France. In France, pavement watering has been conducted every summer since 2013 in Paris when certain meteorological conditions are met (mean 3-day maximum air temperature > 25 °C, wind speed <10 km/h, and sunny skies), relating to the city's heat health warning thresholds (Pascal et al., 2006). Non-potable water is deposited with a cleaning truck at set intervals or via a removable water pipe which continuously supplies water. These events have been extensively studied to characterise the surface and subsurface pavement temperature changes (Hendel and Royon, 2015; Hendel et al., 2015a, 2015b, 2014), as well as to investigate the climate benefits (Hendel et al., 2016; Parison et al., 2020), finding up to 1 °C air temperature reductions and 1–3.5 °C reductions of UTCI. The field experiment results from France, Japan, and Korea are summarised in Table 1. Modelling studies of watering of impervious surfaces have also found cooling benefits. Daniel et al. (2018) simulated a 2100 heatwave in Paris with the Town Energy Balance (TEB) model. Pavement watering induced cooling of up to 1 °C for air temperature at 2 m when simulated from 8 am to 8 pm, with 603 km^2 surfaces being wetted at 1.5GL day^{-1}. In Broadbent et al. (2018), bare soil irrigation was found to have a high irrigation efficiency (in terms of cooling benefit per volume of water) and a suitable method for rapid emergency cooling. Additionally, research on porous pavement has found that strategic wetting can also be effective in reducing surface temperatures under hot and humid conditions with optimal applications between 7 – 11 am (Wang et al., 2022). Modelling of porous pavement has also supported mornings as the optimal wetting times (Kubilay et al., 2021) and identified the ideal weather conditions (Liu et al., 2022) for wetting to support maximum thermal comfort benefits.

Hendel et al. (2020) summaries the general conditions to maximise pavement watering efficiency: the surface is fully exposed to sunlight and enough water is applied to prevent the surface drying while also minimising runoff and drainage, i.e., optimising for evaporation and thus Q_E. The extent of cooling was investigated by Takebayashi et al. (2021), who found that thermal comfort benefits reduce the greater the distance from the wetted surface and the smaller the reduction in surface temperature. For example, the reduction in Standard New Effective Temperature (SET*) decreased from 0.48 °C to 0.24 °C 1 m away from the watered roadway, for a 7.4 °C reduction in surface temperature.

These previous studies provide a basis for pavement watering; however, it is clear that results depend on the specific site locations and prevailing conditions. Indeed, Hendel et al. (2016) notes that a limitation of field studies is the assumption that control and experimental sites are comparable. Pre-existing differences and interactions between sites may cause errors in reported cooling effects, although there have been some attempts to overcome this issue with statistical analysis. Thus, the aim of this study is to assess the cooling impacts and extents of pavement watering through micro-climate observations by conducting a series of experiments in a controlled environment and investigating the impacts on air temperature, thermal comfort, surface temperature, and the surface energy balance.

Table 1

Observed maximum impacts of pavement watering field experiments. GT is Globe Temperature, UTCI is Universal Thermal Climate Index, and SET* is Standard New Effective Temperature.

Study	Measurement Height (m)	Details	Air Temperature (°C)	Humidity (%)	Measure of Thermal Comfort (°C)
Kinouchi (1997)	1	Snow-melting pipes, watering road from 10:00 to 14:00	-1	+4	−4 (GT)
Himeno et al. (2010)	0.9	Snow-melting pipes, 12 L min^{-1} on road for 3 min every 30 min Morning: 8:30 to 10:30	−2	–	–
Himeno et al. (2010)	0.9	Snow-melting pipes, 12 L min^{-1} on road for 3 min every 30 min Afternoon: 17:10 to 19:10	−4	–	–
Hendel et al. (2016)	1.5	Paris 2013–2014 summer field experiments Louvre site: cleaning truck and a manual operator for road and sidewalk 1 mm every hour from 6:20 to 11:30 and every 30 min from 14:00 to 20:30	−0.79	+4.1	−1.03 (UTCI)
Hendel et al. (2016)	1.5	Belleville site: 40 m watering pipe continuously watered pavement at 25 mm h^{-1} from 7:00 to 21:00	−0.60	+1.6	−0.93 (UTCI)
Parison et al. (2020)	1.5	Paris annual summer field experiments, statistical analysis of Louvre site data: 2013–2015 campaign, watering road and sidewalk (100% of street width)	−1.02	+4.08	−1.93 (UTCI)
Parison et al. (2020)	1.5	2016–2018 campaign, watering road only (66% of street width)	−0.97	+3.03	−3.42 (UTCI)
Takebayashi et al. (2021)	1.2	Sufficient water supplied to wet the surface watering one road lane	None[a]	None[a]	−0.8 (SET*)
Takebayashi et al. (2021)	1.2	Watering pedestrian pavement	–	–	−2.5 (SET*)

[a] As only one of multiple lanes were watered, no change in air temperature and relative humidity was observed at 1.2 m, presumed to be due to air mixing.

2. Methods

2.1. Experiment site and design

The experimental program was conducted within the Monash University's Clayton Campus in Australia. Clayton is located in Greater Melbourne, which is characterised as a temperate oceanic climate (Köppen climate classification Cfb) (Beck et al., 2018). The experiment site was located on Level 4 of the North 1 Carpark (37°54′29.44"S, 145°7′52.13″E), where there is an unshaded, flat rooftop and available water.

Figure 1a shows the experimental setup. A 10 m × 10 m plot was established using silicone sealant applied along the perimeter. This area was manually watered, and efforts were made to ensure the entire plot was wet and minimise runoff. Two weather stations were assembled (Fig. 1b) and used alongside Kestrel weather meters. Additionally, a handheld infrared thermometer was used to take transects of surface temperature ($T_{s,trns}$). The second weather station (the control) was positioned upwind, at a right angle to prevailing winds, and at least 5 m from the experimental wetted area before each experiment. See Table 2 for sensor specifications. Weather station dataloggers and Kestrels recorded observations every 30 s. $T_{s,trns}$ measurements were conducted before and after watering, and then at 10-min intervals.

Experiments were conducted on four days in February 2022 (the 7th, 8th, 12th, and 13th). On each of these days, the maximum temperature exceeded 28 °C and there was no precipitation (see Appendix A.1 for the general daily conditions). Data from the first day of experiments (the 7th) was excluded from results due to initial setup errors. Similar to Middel et al. (2021), watering was done at midday (M), in the afternoon (A), and in the evening (E) in an attempt to capture the effects of pavement watering during peak

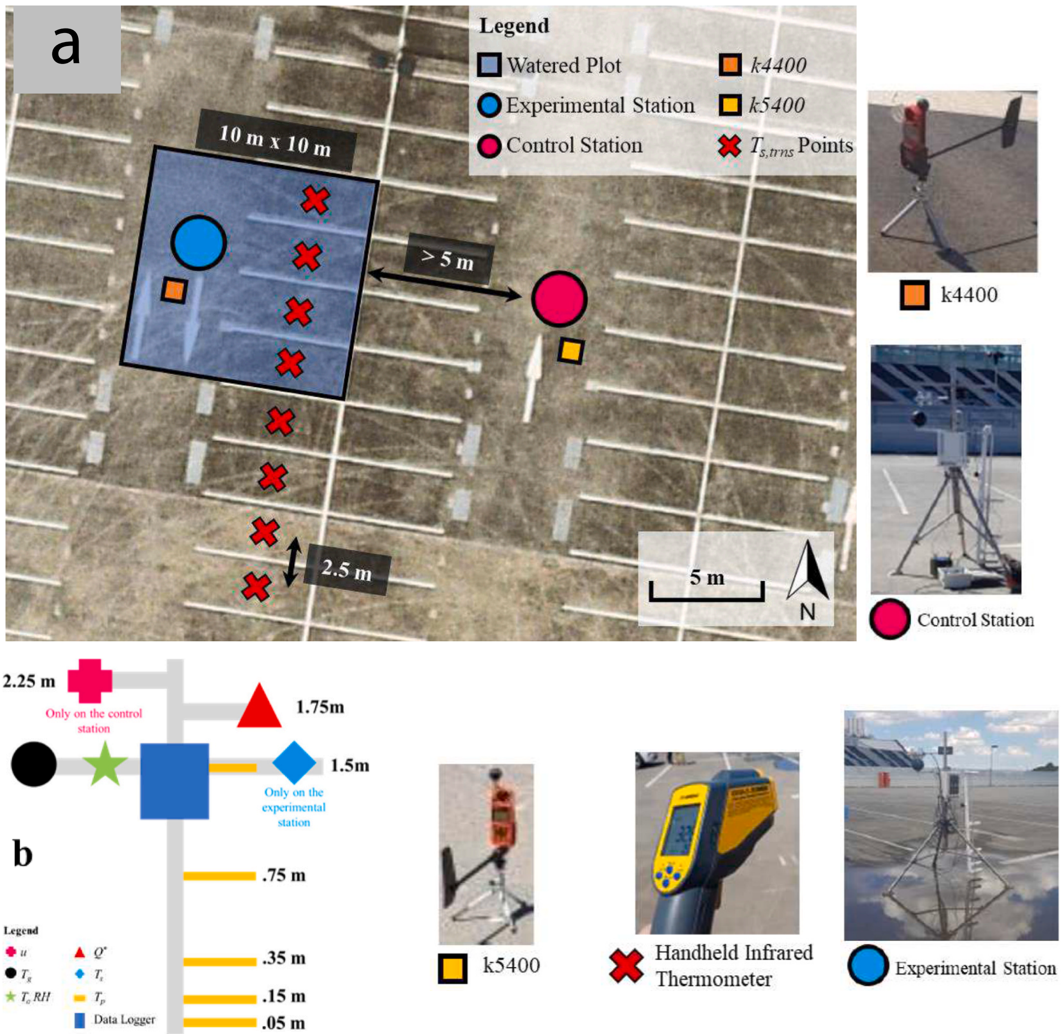

Fig. 1. The experiment site and setup, showing (a) an aerial view of the site (adapted from Nearmap (2022)); and (b) a conceptual diagram of the weather stations. The control station and kestrel (k5400) positions were not fixed, as they were moved to ensure they were upwind of the watered plot. Sensor details are given in Table 2.

Table 2
The sensors used in the pavement watering experiments. The symbols correspond to those used in Fig. 1.

Symbol	Sensor	Model	Variable(s)	Accuracy	Amount	Height(s)
	Anemometer	NRG 40C	Wind speed (u)	Within $0.1ms^{-1}$ (between 5 and $25ms^{-1}$)	1 (control)	2.25 m
	Thermistor within black sphere	Campbell Scientific BlackGlobe	Globe temperature (T_g)	±0.3 °C (between −3 °C to 90 °C)	2	1.5 m
	Temperature and Relative Humidity Probe	Campbell Scientific HMP45C	Air temperature (T_a)	±0.2 °C at 20 °C, ±0.3 °C at 40 °C	2	1.5 m
			Relative humidity (RH)	±2% (0% to 90%)		
	Net Radiometer (with attached thermocouple)	Campbell Scientific CNR1 (Type E thermocouple)	Incoming solar ($K\downarrow$), outgoing solar ($K\uparrow$) Incoming far infrared ($L\downarrow$), Outgoing far infrared ($L\uparrow$) Net radiation (Q^*)	±10% (for the daily totals of each component)	2	1.75 m
	Infrared Radiometer	Campbell Scientific SI-111	Surface temperature (T_s)	±0.2 °C (between −10 °C to 90 °C)	1 (experimental)	1.5 m
	Thermocouple	Type E	Air temperature profile (T_p)	Greater of ±1.7 °C or ± 0.5%	10	1.5 m, 0.75 m, 0.35 m, 0.15 m, 0.05 m
	Handheld Weather Meter	Kestrel 4400 (k4400)	Air temperature (K_T), Relative humidity (K_{RH}), Wind speed (K_u)	±0.5 °C, ±3%, ±0.1 ms^{-1} or 3% of reading	1 (experimental)	0.3 m
	Handheld Weather Meter	Kestrel 5400 (k5400)	Air temperature (K_T), Relative humidity (K_{RH}), Wind speed (K_u)	±0.5 °C, ±2%, ±0.1 ms^{-1} or 3%	1 (control)	0.3 m
	Handheld Infrared Thermometer	Omega O5425-LS	Surface temperature ($T_{s,trns}$)	±1 °C at 20 °C, ±0.3 °C at 40 °C	1	-1 m

incoming solar radiation ($K\downarrow$), peak air temperature (T_a) and air temperature profile (T_p), and after sunset (negative net energy, Q^*) respectively.

Initially, a volume of 100 L was used before being reduced to 60 L to avoid excess runoff. The amounts were chosen to provide sufficient water volume to meet reference evapotranspiration (ETO), approximately 4 mm per day in Melbourne summers. Excess water amounts were not expected to provide additional air temperature reductions as other research, on the irrigation of turf grass, has shown that excess irrigation beyond maintaining soil moisture at field capacity doesn't induce additional reductions beyond reference ETO (Cheung et al., 2022). On the 13th, an additional 20 L of water was applied every 15 min for two experiments to test the impacts of more frequent watering. See Table 3 for a summary of experiments, where each experiment is named after the experiment date and the time of watering.

2.2. *Data processing*

2.2.1. *Sensor validation*

A validation period was conducted to ensure that control and experimental sensors were comparable. To do this, sensors were

Table 3
Experiment details, excluding experiments conducted on the 7th due to setup errors.

Date	Key	Watering Time/s	Watering Amount/s	Notes
08.02.2022	8M	11:40	100 L	Significant water leakage, reached carpark edge
	8A	14:55	100 L	
	8E	19:30	100 L	
12.02.2022	12M	11:58	60 L	Water leakage still present, but more controlled
	12A	15:32	60 L	
	12E	19:30	60 L	
13.02.2022	13M	12:00, 12:15, 12:30, 12:45	60 L (20 L × 3)	Water leakage same the 12th, errors in $T_{p,1.5}$, $T_{p,0.15}$, and T_g that were fixed before 13E
	13A	15:58, 16:15, 16:30, 16:45	60 L (20 L × 3)	
	13E	19:26	60 L	

placed side by side in a lab after the pavement watering experiments. Ideally, sensors should be calibrated before experiments (Phillips et al., 2001), but this was not possible due to preparation being severely impacted by COVID-19 and timing constraints. The Type E thermocouples were not included in the validation period, as they frequently required replacement between experiments. However, as all thermocouples were made from the same cable roll using the same procedure, this was initially considered acceptable. The thermocouples were appropriately shielded but were not ventilated.

The validation period showed that the T_a, RH, K_{RH}, $L\downarrow$, and $L\uparrow$ sensors were not directly comparable. The T_a readings showed several unnatural readings during the experiment and validation period (e.g., $-40\,^\circ$C), and thus was discarded in favour of $T_{p,1.5}$, which also captured air temperature at 1.5 m. For RH andK_{RH}, the mean difference between the sensors was calculated and applied to the data.

The internal net radiometer $L\downarrow$ and $L\uparrow$ calculations consider the measured sensor temperature (T_{CNR1}). It was found that the difference in T_{CNR1} was causing the inconsistencies in $L\downarrow$ and $L\uparrow$ readings. Subsequent tests showed that it was likely that the experimental T_{CNR1} sensor was inaccurate. Therefore, it was assumed that the actual T_{CNR1} did not vary between the control and experimental sensors, thus $L\downarrow$ and $L\uparrow$ was corrected by recalculating them using the control sensor temperature. Some small differences are expected in observed $K\uparrow$ due to differing albedo between dry weathered asphalt and wet asphalt, 0.15–0.20 vs.0.18 (Sandia National Laboratories, 2024). These differences are expected to be smaller than the accuracy of the sensor. More details on the validation period and corrections can be found in Appendix A.2.

2.2.2. Derived variables

Additional variables were derived based on the observed data acquired from the experiments, namely wind speed at 10 m (u_{10}), surface temperature ($T_{s,drvd}$), vapour-pressure deficit (VPD), mean radiant temperature (T_{MRT}), Universal Thermal Climate Index (UTCI, a widely used measure of heat stress in outdoor spaces (Zare et al., 2018)), and components of the surface energy balance (SEB).

The wind profile power law (Manwell et al., 2010; Bañuelos-Ruedas et al., 2010) was utilised with u and K_u to derive u_{10} (Appendix A.3.1). The relationship between T_s and $L\uparrow$ (Oke et al., 2017) was used to calculate $T_{s,drvd}$ (Appendix A.3.2). VPD was calculated using $T_{p,1.5}$ and RH (Allen et al., 1998; McMahon et al., 2013) (Appendix A.3.3). The python library pythermalcomfort (Tartarini and Schiavon, 2020) was used to calculate T_{MRT} and UTCI, the former using T_g, $T_{p,1.5}$, and u_{10}, and the latter using $T_{p,1.5}$, T_{MRT}, RH, and u_{10} (Appendix A.3.4).

The SEB was also calculated. It can be simplified as:

$$Q^* = Q_H + Q_E + \Delta Q_S \tag{1}$$

where Q^* is the net all radiation (Wm^{-2}) (i.e., ($K\downarrow$-$K\uparrow$) + ($L\downarrow$-$L\uparrow$)), Q_H is the sensible heat flux (Wm^{-2}), Q_E is the latent heat flux (Wm^{-2}), and ΔQ_S is the change in heat storage (Wm^{-2}) (Oke et al., 2017). The mean Q_E from the start of watering to the approximate drying time was estimated based on the amount of water and the approximate evaporation time. Q_H was calculated based on $T_{s,drvd}$, $T_{p,0.05}$, and u_{10} (Liu et al., 2007), as well as roughness lengths from Kanda et al. (2007), while Q^* was directly measured. The mean Q_H and Q^* from the wet period was calculated, allowing the mean ΔQ_S to be estimated as the energy balance residual (Oke et al., 2017). These mean values were also used to calculate the Bowen ratio ($\beta = Q_H/Q_E$) alongside the ratio of Q_H to Q^* (Q_H/Q^*) (Oke et al., 2017). See Appendix A.3.5 for details.

2.2.3. Statistical analysis

The difference between the control and experimental sites was calculated (Δ = experimental - control, thus $\Delta < 0$ indicates cooling). Preliminary analysis showed that even after applying corrections to account for incompatible sensors, differences between the control and experimental variables still existed before watering took place. These differences varied between the experiments and observational variables, and are explored with more detail in the results. As the expected impact of watering is small, these relatively small pre-existing differences can exaggerate or diminish the actual impact of pavement watering, depending on the initial bias.

Thus, for the purposes of this study, impacts were assessed by evaluating changes relative to the initial difference. Specifically, the average difference between the control and experiment before watering ($\overline{\Delta}_{dry}$), taken as a maximum of 30 min before watering, was compared to the average difference during the wet period ($\overline{\Delta}_{wet}$), which was defined as when watering was finished to when it was dry under the experimental station (for experiments with repeated applications of water, the end of the initial watering was used). In other words, the observed cooling impact of pavement watering (PW_{impact}) in a particular experiment was defined as:

$$PW_{impact} = \overline{\Delta}_{wet} - \overline{\Delta}_{dry} \tag{2}$$

A linear mixed effect model was used to verify if $\overline{\Delta}_{wet}$ was significantly lower (or significantly greater for RH) than $\overline{\Delta}_{dry}$. The effect of prevailing conditions on the effectiveness of pavement watering was also explored. To do this, the PW_{impact}, as well as Q_E, were compared to the mean of prevailing conditions during the wet period via linear regression. The statistical significance of a non-zero slope was calculated. For the surface temperature transects ($T_{s,trns}$), the difference between the mean of the watered points and non-watered points was calculated (i.e., $\Delta T_{s,trns} = \overline{T}_{s,trns,wet} - \overline{T}_{s,trns,dry}$), and an analysis of covariance (ANCOVA) was used to verify if the watered points were significantly less than non-watered plots. A p-value of <0.05 was used to validate significance in all cases.

3. Results

3.1. Air temperature profile

An air temperature profile, comprised of temperature observations at five heights (0.05 m to 1.5 m), was measured at the experimental and control site (T_p, see Fig. 1b). The difference was calculated between the temperatures of the same height (ΔT_p). Air temperature at a specific height is referred to as $T_{p,height}$ and likewise differences at a specific height is referred to as $\Delta T_{p,height}$.

As detailed in Section 2, there were differences between the experimental and control T_p before watering was conducted (i.e., $\Delta T_p \neq 0$ before watering). The ΔT_p before watering was found to be variable between the experiments and the different T_p heights. In the evening experiments, ΔT_p was predominantly less than zero, indicating that the experimental site already was cooler than the control site before watering, while midday and afternoon experiments had a mixture of both less and greater than zero (Fig. A.9). Given the apparently random nature of these pre-existing differences at different heights, it is likely they are not reflective of the actual temperature differences between the sites.

The relationship between pre-existing differences and the absolute control temperature ($T_{p,con}$) as well as wind speed (u_{10}) was investigated. The ΔT_p before watering was found to have a statistically significant relationship with $T_{p,con}$ for each individual experiment and height, apart from experiment 13E at 1.5 m (Fig. A.10). A relationship with u_{10} was also found, however it was not as consistently statistically significant (Fig. A.12). There were no significant relationships when considering all the experimental data together, likely as T_p sensors frequently malfunctioned and were replaced, and as the control station was moved to ensure it remained upwind of the watered plot. Thus, ΔT_p was detrended based on the linear relationship derived for each individual experiment and height in an attempt to remove factors that caused the observed differences between sites that were unrelated to pavement watering. However, it was found that results were biased by the changes in $T_{p,con}$ and u_{10} values throughout the experiment.

Figure 2 highlights these issues with an example of observed temperature differences for experiment 12M at 0.15 m. The $\Delta T_{p,0.15}$ was already less than zero before watering, and thus the cooling of pavement watering would be exaggerated if simply taken as the difference between the experimental and control site when the surface is wet (Fig. 2c). Despite this, there was still a clear negative shift in $\Delta T_{p,0.15}$ when the surface was wet, indicating that pavement watering may have a cooling effect. Thus, it was possible to derive the impact of pavement watering by simply shifting the observed differences based on the mean of the before watering period, however this assumes that the pre-existing differences were constant (Fig. 2c).

The linear relationship between the pre-existing $\Delta T_{p,0.15}$ and $T_{p,con}$ at the same height is shown in Fig. 2a ($p < 0.01$), and the $\Delta T_{p,0.15}$ detrended with this relationship is shown in Fig. 2c. This corrected $\Delta T_{p,0.15}$ shows a positive shift in differences after watering (i.e., the experimental site becoming warmer than the control). However, this was likely due to temperatures increasing throughout the midday experiment, beyond the values used to calculate the applied linear model. As higher temperature was related to a more negative $\Delta T_{p,0.15}$, the corrected $\Delta T_{p,0.15}$ reflected the change in $T_{p,con}$ relative to before watering rather than isolating the impacts of pavement watering. This was also seen as the detrended ΔT_p based on $T_{p,con}$ generally showed no cooling from pavement watering for midday experiments where temperatures increased through the experiment, and high cooling for evening experiments where temperature progressively decreased (Fig. A.11).

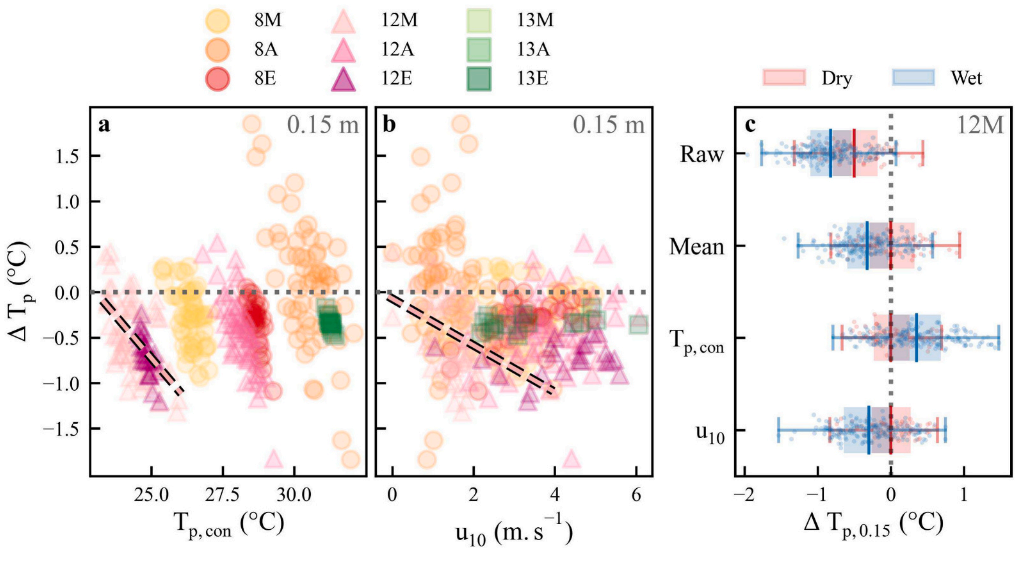

Fig. 2. A scatter plot of before watering ΔT_p vs (a) $T_{p,con}$ and (b) u_{10} for each experiment at 0.15 m, with the pink line outlined in black showing the linear relationship for experiment 12M. (c) Boxplots of ΔT_p for dry (before watering) and wet periods of experiment 12M at 0.15 m with different corrections applied (raw: no correction, mean: shifted based on dry mean, $T_{p,con}$: detrended based on linear relationship in (a), u_{10}: detrended based on linear relationship in (b).

The same problems were seen when correcting ΔT_p based on its relationship with wind speed. Fig. 2b shows the linear relationship between pre-existing $\Delta T_{p,0.15}$ and u_{10} ($p < 0.01$), and the corresponding corrected $\Delta T_{p,0.15}$ is shown in Fig. 2c. The corrected $\Delta T_{p,0.15}$ is somewhat similar to correcting $\Delta T_{p,0.15}$ based on the mean of the pre-existing differences. The shift in u_{10} values before and after watering was not as acute as with $T_{p,con}$, however it still likely leads to unintended side-effects, including increasing the variability of $\Delta T_{p,0.15}$ when it is wet.

Thus, to avoid the uncertainties associated with the extrapolation of the calculated linear models, the ΔT_p relative to the mean before watering was chosen to assess the impacts of pavement watering. Fig. 3 shows the mean corrected ΔT_p for experiment 8M. The corrected ΔT_p shows that watering generally had a decreasing impact with increasing height. There also was an immediate cooling effect, especially at lower heights. After the surface dried, some temperature differences returned to the established baseline (the mean of the before watering differences) generally within an hour, however they also often increased, or decreased, relative to the baseline. This can be seen in both Fig. 2b as well as the other experiments (Fig. A.14). It is difficult to be certain of the long-term effects given the apparent instability of the measured differences between the control and experimental site, and thus the true impact of pavement watering.

To overcome these challenges and uncertainties, the cooling impact of pavement watering on air temperature was taken as the mean difference during the wet period relative to the mean difference before watering (i.e., PW_{impact} for T_p, see Eq. 2). The PW_{impact} for T_p varied from no observable decrease to a cooling of up to 1 °C, with the exception of 2.5 °C at 0.05 m for experiment 8A (Fig. 4a). Consistent with Fig. 4b, cooling generally decreased with height (Fig. 4a). Considering all experiments, the evening experiments had the lowest air temperature cooling at 0.05 m, however there was no clear decrease in cooling for evening experiments at other T_p heights. However, considering individual experiment days, the cooling was generally greatest in the afternoon and lowest in the evening, especially at lower heights.

Given the spread in results, the specific conditions during individual experiments were investigated. Namely, as pavement watering utilises evaporative cooling, firstly the impact of prevailing conditions known to influence Q_E was explored (Fig. 4b). Q_E was found to be positively correlated to u_{10} ($p < 0.01$, $R^2 = 0.74$), and also related to experimental VPD and Q^* ($R^2 = 0.31$ and 0.15 respectively), although these relationships were not statistically significant ($p = 0.15$ and 0.30 respectively) (Fig. 4). As expected, Q^* was found to be highly correlated to $K\downarrow$ ($R^2 = 0.99$), suggesting that solar radiation was a key source of energy for Q_E.

However, there was no strong correlation between air temperature cooling and Q_E. Q_E had a slight positive correlation with air temperature cooling at 0.75 m ($R^2 = 0.11$) and 0.35 m ($R^2 = 0.01$), a weak negative relationship at 1.5 m ($R^2 = 0.07$) and 0.15 m ($R^2 = 0.05$), and no impact at 0.05 m ($R^2 < 0.01$). Additionally, none of these relationships were statistically significant ($p > 0.4$) (Fig. 4c-g). The weak negative relationship at 1.5 m and 0.15 m was likely due to the malfunctions at those heights for experiment 13M and 13A, which had high Q_E and low cooling at other heights. Thus, high Q_E was marginally related to reduced air temperature cooling.

On the other hand, air temperature cooling was found to be related to wind speed. Lower u_{10} related to more cooling across all T_p heights (R^2 ranged from 0.15 to 0.36), although again these relationships were statistically insignificant ($p > 0.09$) (Fig. 4c-g).

Air temperature was also recorded at 0.3 m with the Kestrels (K_T) (Fig. 1a). However, this was impacted by rather extreme pre-existing differences, with ΔK_T before watering found to be up to 6 °C. Additionally, the PW_{impact} for K_T (Eq. 2) did not align with results from the temperature profile, with a maximum cooling of 0.84 °C (13A) and maximum warming of 0.61 °C (13M) (Table A2).

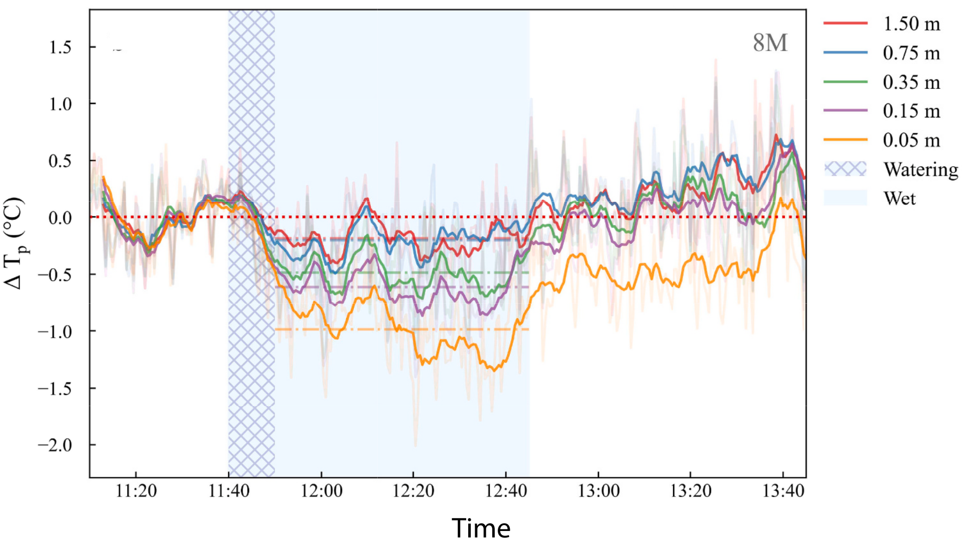

Fig. 3. T_p differences for experiment 8M with corrections based on the mean of before watering. The transparent lines represent the raw data, while the solid lines are the 5-min running average. The shading indicates periods when the pavement was wet, and the hatching shows when watering was being conducted. The dashed lines represent the mean of the wet period.

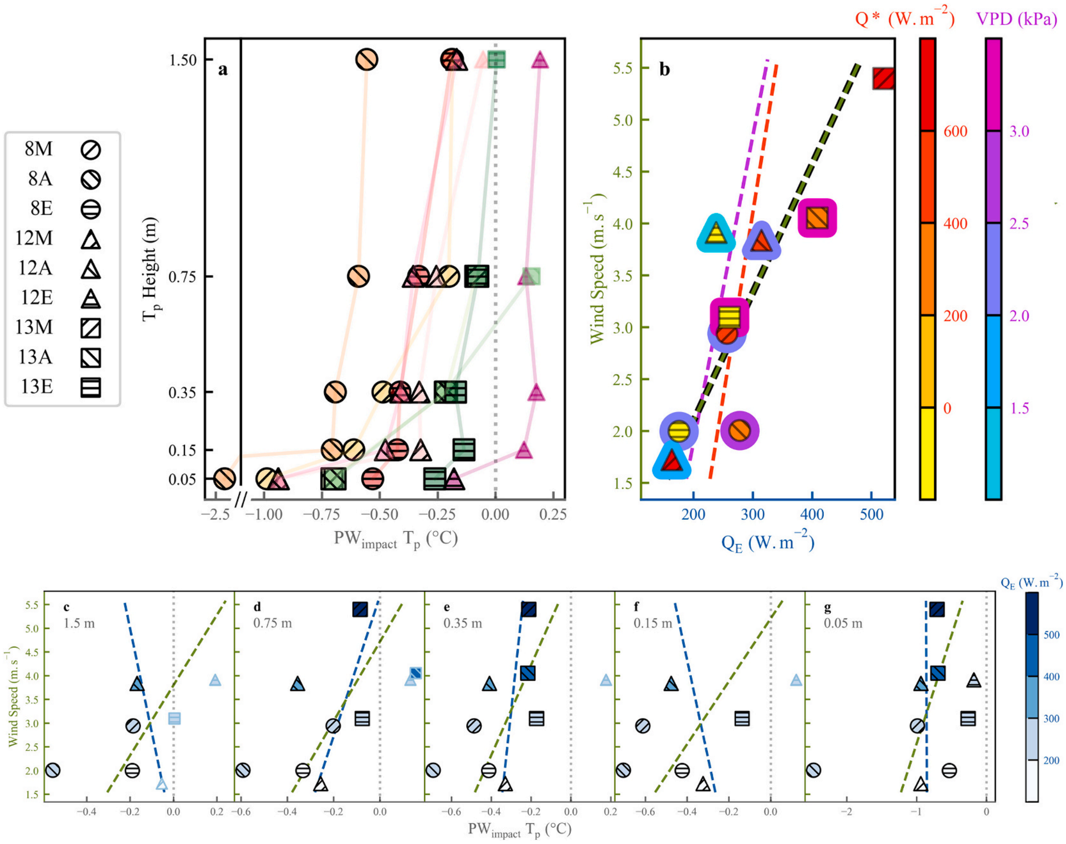

Fig. 4. (a) The PW_{impact} for T_p at each T_p height, where each scatter marker colour indicates a separate experiment. Note the x-axis is discontinuous. (b) the relationship between Q_E and the mean u_{10} (y-axis, green dashed line), the experimental Q^*, (red dashed line, colour of scatter marker) and the experimental VPD (purple dashed line, border colour of scatter marker) during the wet period; (c-g) PW_{impact} for T_p vs u_{10} y-axis, (green dashed line) and Q_E (blue dashed line, colour of scatter marker) at each T_p height. A black outline for the scatter points indicates a statistically significant change in T_p (a, c-g), while a black outline on the dashed line indicates a statistically significant linear relationship (b, c-g). (For interpretation of the references to colour in this figure legend, the reader is referred to the web version of this article.)

Although the Kestrels were tested in the validation period and appeared to be compatible (Appendix A.2), the two Kestrels may have responded differently in the relatively dynamic, hot carpark environment, especially when compared to a lab environment. Thus, these results are disregarded given that two different Kestrel models were potentially inappropriate for the purposes of this experiment.

Overall, pavement watering was found to reduce air temperature, with a maximum decrease of 0.6 °C and 2.5 °C found at 1.5 m and 0.05 m respectively. Despite the uncertainties associated with the differences between the control and experimental observations, the derived impact of pavement watering on air temperature was within estimates from other field studies (see Table 1), and indeed align with expectations, for example decreased cooling with height. The impact of pavement watering was also found to be dependent on prevailing conditions, especially wind speed, but was not found to be strongly correlated with Q_E.

3.2. Thermal comfort

The thermal comfort benefits of pavement watering was assessed using UTCI. This, as well as T_{MRT}, was calculated with observational $T_{p,1.5}$, RH, T_g, and u. As detailed above, the air temperature at 1.5 m was significantly different between the control and experimental station before watering took place. RH and T_g also had pre-existing differences, and like T_p, this varied with the experiments. Nevertheless, these observations were used to calculate T_{MRT} and UTCI, and thus these variables also inherited pre-existing differences. Thus, as with air temperature, the PW_{impact} (Eq. 2) was used to derive the impact of pavement watering.

The PW_{impact} for UTCI and all its components, save wind speed, which was considered the same across the entire carpark, is shown in Fig. 5. UTCI was found to be reduced by 0.2 °C to 2.0 °C by pavement watering, despite watering generally increasing RH (−0.02% to 1.19%). It should be noted that spikes in RH were seen at the experimental site after watering, which was not captured by the PW_{impact}.

T_{MRT} was found to drive UTCI changes, except in experiments 12M and 12E where there was little observable air temperature cooling. As with air temperature, for individual experiment days, the UTCI reduction is greatest in the afternoon and lowest in the

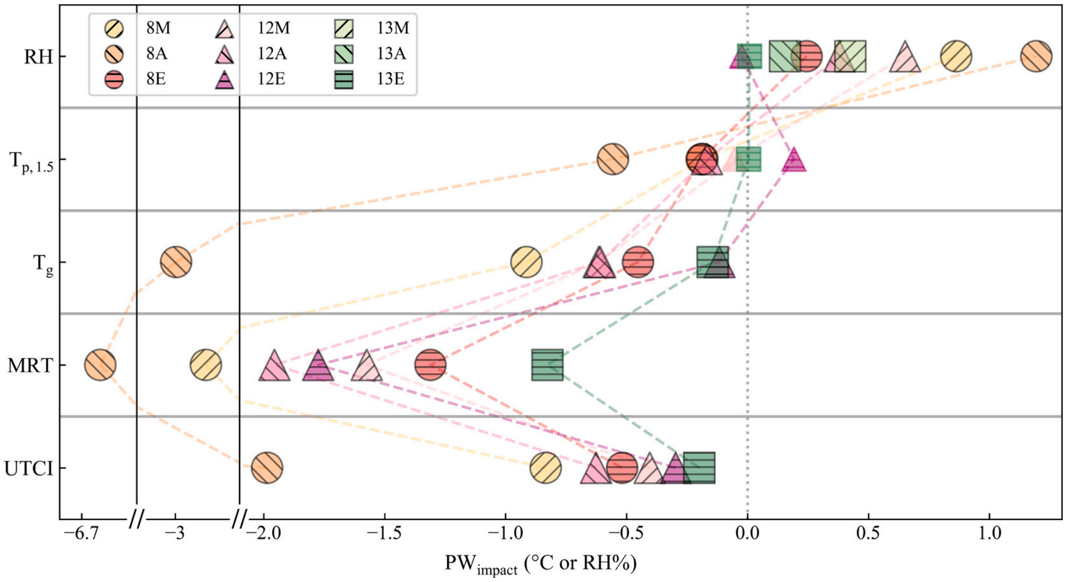

Fig. 5. The PW_{impact} for UTCI and its variables (RH, $T_{p,1.5}$, T_g, and T_{MRT}) for each experiment. The black outline indicates a statistically significant impact from watering for a particular variable ($p < 0.05$). Note the x-axis is discontinuous.

evening. Reduction in T_{MRT} due to watering is weakest during the evening, which also leads to a lower UTCI reduction in the evening. In summary, pavement watering was found to improve thermal comfort. Despite observed increases in RH, reductions in air temperature and globe temperature resulted in reducing UTCI by a maximum of 2.0 °C.

3.3. Surface temperature

The surface temperature was measured via transects ($T_{s,trns}$) with one handheld infrared thermometer, with 4 points outside the designated watered plot and 4 within (Fig. 1a). A single transect was done before watering, allowing for the investigation of actual differences within the sites before watering takes place. Additionally, surface temperature was derived ($T_{s,drvd}$) for the control and experimental station using $L\uparrow$ and verified with observations from the one available continuous surface temperature sensor on the experimental station. $\Delta T_{s,trns}$ refers to the difference between the mean surface temperature of the watered points and the mean of the non-watered points, while $\Delta T_{s,drvd}$ refers to the difference between the experimental and control derived surface temperature.

Figure 6 shows the surface temperature transects for experiment 13E, alongside the $\Delta T_{s,trns}$ for all experiments. Both these figures show that watering resulted in a clear reduction in surface temperature. This cooling remained significant even after the surface visibly dried for all experiments, excluding 8M, 13A, and 13E. Additional independent t-tests between the control and experimental points

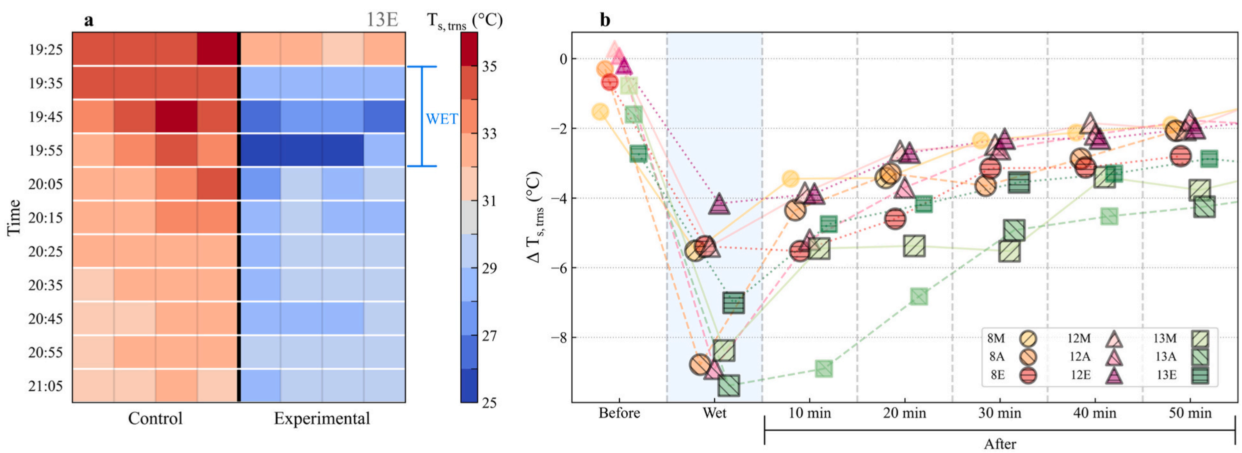

Fig. 6. (a) The $T_{s,trns}$ of experiment 13E showing the evolution from before, during, and after the wet period (rows) for control and experimental points along the transect (columns); (b) the $\Delta T_{s,trns}$ of all experiments, where the wet refers to the mean $\Delta T_{s,trns}$ of the wet period. The black outline indicates that the experimental points are statistically significantly lower than the control points ($p < 0.05$).

before watering showed that these three experiments (8M, 13A, 13E) were significantly different, while differences in the other experiments were insignificant. The heterogeneity of the carpark surface is apparent in Fig. 6a. The greatest difference within the control points for the same transect was 3.8 °C (12A), and 8.4 °C (8A) for experimental points (Fig. A.15), the latter potentially due to the different drying rates across the watered plot.

It is also evident that $\Delta T_{s,trns}$ was usually less than zero before watering, and this difference was statistically significant for three experiments (Fig. 6b). With the exception of experiment 8M, the magnitude of these before watering differences increased throughout the day (e.g., 13M < 13A < 13E) (Fig. 6b). This suggests that the effect of watering lasted beyond a given experiment, and has a long-lasting cooling impact on surface temperature. This is also shown in the derived surface temperature, where there was little differences between control and experimental sites before the midday experiment (−0.2 °C to −0.5 °C), followed by a significantly cooler experimental surface temperatures before the afternoon (−1.7 °C to −2.2 °C) and evening (−1.8 °C to −3.4 °C) experiments (Fig. A.17 and Table A3).

In an attempt to isolate the experiments, the $\Delta T_{s,trns}$ was also calculated relative to the transect done before watering. A mean decrease of 4.0 °C to 9.0 °C was observed during the wet period for the isolated experiments (Fig. A.16). The raw mean decrease in surface temperature can be taken as the cumulative impact of pavement watering, and this was slightly higher (4.2 °C to 9.3 °C) (Fig. 6b).

As derived surface temperature was observed regularly, the impact of pavement watering for each individual experiment can be derived with PW_{impact} (Eq. 2). Pavement watering decreased $T_{s,drvd}$ by 2.1 °C to 6.8 °C, however it should be noted that experimental $T_{s,drvd}$ does not completely capture the minimum surface temperature observations (as measured by the observational T_s sensor), and thus these results are likely underestimated (Fig. A.17 and Table A3). Similar to the $\Delta T_{s,trns}$, the cumulative impact of watering on surface temperature can be taken as the mean during the wet period without any corrections. The cumulative decrease seen in $T_{s,drvd}$ was 3.7 °C to 7.3 °C (Fig. A.17 and Table A3).

In all measures of surface temperature, there was generally lower individual reductions in the evening experiments, although this was partially compensated with the cumulative cooling from previous experiments. The highest individual and cumulative cooling was seen in the afternoon, likely as the experimental surface reached its peak temperature in the period before the afternoon experiment (Fig. A.17 and Table A3).

In general, the surface temperature cooled by up to 9.0 °C due to pavement watering. The watered surface remained noticeably cooler than the non-watered surface even after the water visibly dried, and likely led to cumulative cooling for each subsequent experiment within the individual experiment days. Thus, pavement watering was shown to significantly reduce surface temperature when wet and have a prolonged cooling effect even after the surface dried.

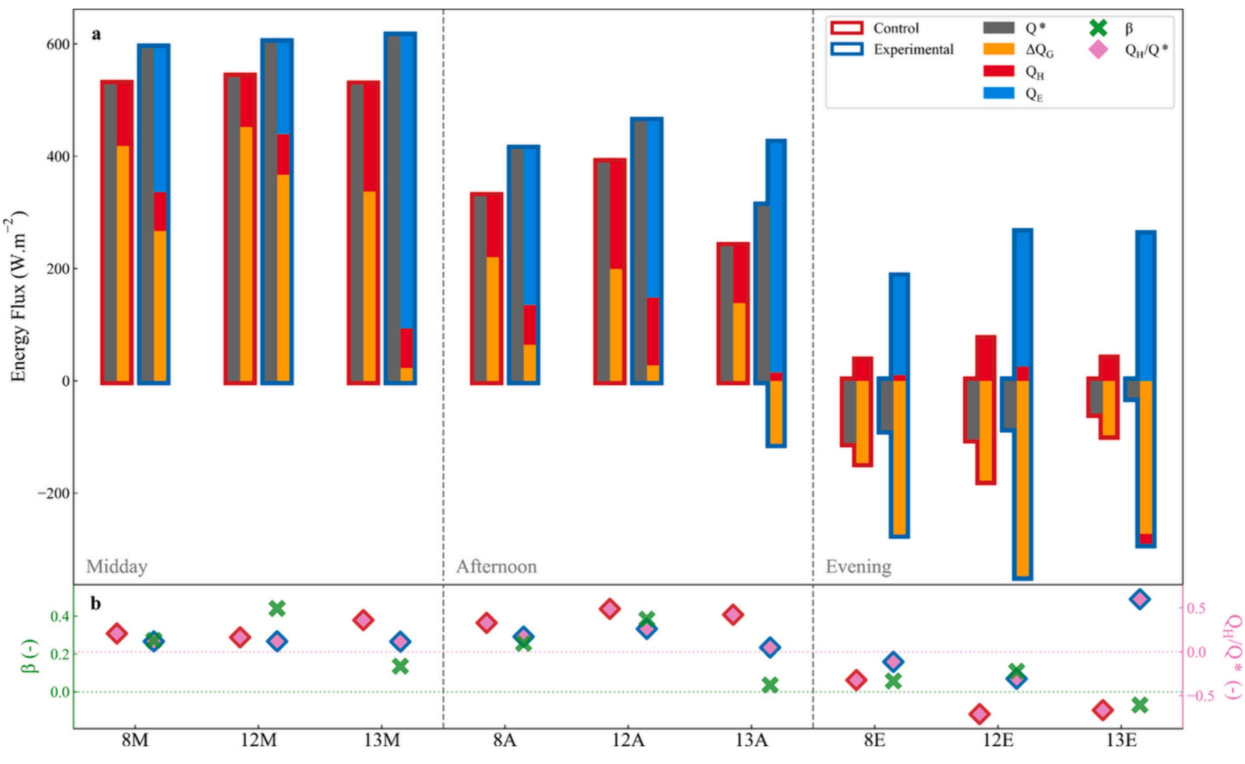

Fig. 7. (a) The mean SEB of each experiment's control and experimental site during the wet period; (b) the β alongside the Q_H and Q^* ratio for each experiment.

3.4. Surface energy balance

The surface energy balance (SEB) was simplified to net radiation (Q^*), latent heat flux (Q_E), sensible heat flux (Q_H), and change in heat storage (ΔQ_S). Q^* was directly observed, while Q_E and Q_H where calculated, the latter based largely on the derived surface temperature ($T_{s,drvd}$) and air temperature at 0.05 m ($T_{p,0.05}$). Finally, ΔQ_S was derived as the SEB residual. Fig. 7a shows the mean SEB during the wet period at the control and experimental site for each experiment. There is a marked impact of watering, namely the presence of Q_E, higher Q^*, and lower Q_H and ΔQ_S.

It was found that surface albedo and temperature decreased due to watering, leading to decreased $K\uparrow$ and $L\uparrow$, and thus higher Q^*. Q_E more than compensates for this increase in Q^*, as a large portion of Q^* appears to be forcing Q_E for midday and afternoon experiments, while energy is predominantly provided by ΔQ_S in the evening. ΔQ_S was also notably negative for experiment 13A, and Q_H was negative for 13E, suggesting that they also contributed to Q_E.

Figure 7b shows the Bowen ratio (β) alongside the Q_H to Q^* ratio (Q_H/Q^*) for each experiment. The β ranges from 0.04 to 0.44 during the day, and from −0.07 to 0.11 in the evening. A daytime β of 0.1 to 0.3 is typical of a tropical wet forest, while a β of 3 to 8 is associated with urban areas with <20% greenspace (Oke et al., 2017). Thus, it is evident that the addition of water allows the otherwise dry carpark, characteristic of an urban area, to imitate highly evaporative environments.

The difference between the experimental and control Q_H/Q^* (i.e., the $\Delta Q_H/Q^*$) ranges from −0.05 to −0.37 in the midday and afternoon experiments (Fig. 7b), indicating that less Q^* was partitioned into Q_H due to watering despite increased Q^*. For the evening experiments, $\Delta Q_H/Q^*$ ranged from 0.21 to 1.27 (Fig. 7b). This indicates that the control site had a lower Q_H/Q^*, which is expected as Q^* is negative, and thus still relates to a decreased Q_H at the watered site.

It should be acknowledged that existing differences before each experiments impacted the SEB and Q_H/Q^*, as $T_{s,drvd}$ and $T_{p,0.05}$ both had differences between the control and experimental site before watering, as discussed in previous sections. Analysis of the SEB in the period before watering reflected these pre-existing differences between the sites, especially for afternoon and evening experiments (Fig. A.18). Thus, the actual impact of watering on $\Delta Q_H/Q^*$ can be deduced from the relative change from the $\Delta Q_H/Q^*$ before watering. This difference ranged from −0.04 to −0.24 in the midday and afternoon, and from −0.03 to 1.17 in the evening (Fig. A.19). Thus, watering still resulted in a lower proportion of Q_H, except for experiment 8E, where there was little change relative to before watering took place.

However, these pre-existing differences in the SEB were largely related to the prolonged impact of watering on surface temperature (i.e., differences between the experimental and control $T_{s,drvd}$ rather than $T_{p,0.05}$). This can be seen as the wet period $\Delta Q_H/Q^*$ at midday matches fairly well with the before watering $\Delta Q_H/Q^*$ in the afternoon for all experiment days (e.g., 13M $\Delta Q_H/Q^*$ when wet was close to 13A $\Delta Q_H/Q^*$ before watering), highlighting the effect of prolonged cooling of the surface temperature on the SEB (Fig. A.19). Thus, as with surface temperature, the $\Delta Q_H/Q^*$ during the wet period can be taken as the cumulative impact of pavement watering (Fig. 7b), while the $\Delta Q_H/Q^*$ relative to before watering can be assumed to be the individual experiment impact.

Overall, pavement watering had a considerable impact on the SEB of the carpark. The expected characteristics of a carpark (high Q_H and ΔQ_S) were seen at the control site, while the SEB for the watered section was dominated by Q_E, which is more typical of moist environments. The changes in the SEB are the driving force behind the observed cooling provided by pavement watering.

4. Discussion

As noted above, a key confounding factor of this study stems from the existing differences in the experimental and control observations before watering took place. Given the apparent heterogeneity of the carpark surface (Figs. 6a and A.15), it appears that there may have been slight actual differences between the sites. Moreover, experiments were not as independent as initially assumed, as both the surface temperature transects and the derived surface temperature showed a prolonged cooling due to pavement watering after the surface visibly dried (Figs. 6 and Fig. A.17 and Table A3). However, pre-existing differences for other observations were less stable, for example the differences between the control and experimental air temperature profile changed between experiments and heights (Fig. A.9).

These differences between the control and experimental air temperature observations were negatively correlated to the absolute control observations at an individual experiment level (Fig. A.10), suggesting that the temperature sensors had different sensitivities. Wind speed may have also impacted the control and experimental observations in some experiments (Fig. A.12), indicating that potentially the temperature sensors were not secured properly. However, attempts to isolate and remove these factors that contributed to these differences resulted in the corrected data reflecting changes in observed control temperature and wind speed, rather than potential impacts of watering (Figs. A.11 and A.13).

Therefore, the impact of pavement watering was deduced by comparing differences relative to the mean of the dry period. This is still not ideal, as it involves assuming that the 'natural' difference during an experiment remains stationary. However, this was considered necessary, as using uncorrected data would result in overestimating or underestimating the impact of watering, depending on the initial bias. Indeed, given the alignment of results, for example the cooling impact decreasing with temperature height, it is considered an adequate representation of the impact of pavement watering.

Our experiments were unable to confirm whether cooling impacts are dependent on wind speeds, due to weak correlations in our results, a small observational area being watered, and a lack of observations downwind. Hendel et al. (2015a) only conducted their experiments on days where wind speeds were $<2.8ms^{-1}$ and recommended pavement watering to be most useful to reduce thermal stress on heat wave days, days of Pasquill atmospheric stability classes A or A-B (Pasquill, 1961), where wind speeds are $<3ms^{-1}$ (Hendel et al., 2016). There is a possibility that advection caused a downwind propagation of cooling, as observed in urban parks (Motazedian et al., 2020), and some of the cooling magnitudes we observed in our experiment were lost downwind.

In terms of watering time, evening experiments generally had the lowest observed cooling benefits, particularly for surface temperature, the air temperature closest to the ground ($T_{p,0.05}$), and T_g; and thus, T_{MRT} and UTCI by relation. The relatively low reductions in surface temperature arguably occurred as the carpark surface was already cooling down due to the lack of $K\downarrow$, and likely influenced evening $T_{p,0.05}$ and T_g. Indeed, Takebayashi et al. (2021) found that the cooling effect of pavement watering on surface temperature was generally greater the hotter the surface temperature was, which was also reflected in this study. However, there does not appear to be a clear relationship between surface temperature and air temperature other than at 0.05 m in the evening, potentially due to the stronger heat turbulence during the day and the evident influence of horizontal advection.

Despite the lower cooling benefits, pavement watering may provide key benefits in the evening. Namely, there was a negative Q_H in experiment 13E, while all other evening experiments had a positive Q_H. This likely occurred due to the prolonged cooling impact pavement watering had on surface temperature, which meant that before watering for experiment 13E, Q_H was already lower at the experimental site compared to the control. Additionally, the previous experiments of the day, 13M and 13A, had small and negative ΔQ_S respectively, indicating that the accumulation of heat storage in the ground that is typical of urban surfaces (Oke, 1982; Anandakumar, 1999) was severely limited by pavement watering. This in turn was likely due to the fact that both experiments were characterised by high Q_E, due to both ideal evaporation conditions (high wind speed and VPD) and the extra water that was applied for these experiments. Thus, the previous watering throughout the day may have allowed the reversal of Q_H when watering was applied in the evening. This implies that frequent watering in the right conditions may allow urban areas to cool more effectively at night, and thus mitigate the negative health impacts of high night-time temperatures characteristic of urban areas (Clarke, 1972; Coutts et al., 2010).

However, it should be noted that numerous assumptions were made to calculate the SEB. Notably, ΔQ_S was calculated indirectly and any advection of energy was ignored. Additionally, in an effort to ensure our measurements in this small scale experiment were within the zone of influence of wetting, and by utilising a close to the surface $T_{p,0.05}$ in the Q_H calculation, there might be some underestimation of Q_H and overestimation of ΔQ_S. Despite this, the Cohard et al. (2018) study on the energy budget of a carpark under simulated rainfall events, with appropriate sensors to directly measure ΔQ_S and Q_H, observed the former providing energy for Q_E during the day and latter becoming negative at night, which aligns with results. The overall SEB results are considered valid, but as indicative of the surface energy balance and estimates only.

The cooling benefits of pavement watering found can also be compared to other studies. A study on pavement watering in Paris found a reduction of up to 1 °C in air temperature and 3.4 °C in UTCI at 1.5 m (Parison et al., 2020). This is comparatively higher than the maximum reduction in 1.5 m air temperature and UTCI found in this study, which was 0.6 °C and 2.0 °C respectively. The key difference is that the study in Paris examines the observations of a street that is watered when specific conditions are met, using data from the summers of 2013 to 2018 (Parison et al., 2020), while this study is limited to a small 10 m × 10m plot and three days of experiments.

Thus, a crucial limitation of this study is the small-scale of the experiment, which may have restricted the observed cooling benefits and exaggerated the influence of wind. Several assumptions were also made to calculate variables, and indeed to extract the impact of pavement watering itself. A potential improvement to this study would be to appropriately calibrate the instruments before the experiment, and perhaps a preliminary site assessment, as this may have prevented the need for corrections.

Despite limitations, the benefits of pavement watering were still found to agree with the existing literature. Namely, it is relatively simple to apply in highly urbanised areas and induces a fast-cooling response in the right conditions. For example, in France, pavement watering is conducted via cleaning trucks assisted by manual operators (Hendel et al., 2014). Although this study found relatively small reductions, pavement watering still may provide significant outcomes. Nicholls et al. (2008) showed that in Melbourne, higher mortality of those over 64-years-old is correlated to higher mean daily temperatures once 30 °C is exceeded (calculated as the mean of the day's maximum temperature and the night's minimum temperature). This suggests that even small reductions in both daily and night-time temperature can potentially reduce mortality.

On the other hand, the cooling is highly localised and although there may be relatively small enduring reductions in surface temperature, the limited storage capacity of pavements means that frequent application of water is necessary to sustain benefits.

Moreover, urban heat mitigation techniques should ideally improve a range of social, environmental, and economic outcomes on long-term basis. Pavement watering can be a permanent solution, depending on the type of supporting infrastructure used, as well as provide multiple benefits. For example, in Korea, pavement watering instalments are used to melt snow on roads, discharge water from underground subway systems, and reduce air pollution (Kim et al., 2014; Na et al., 2021). This highlights the additional value provided by pavement watering, where other issues are simultaneously targeted alongside urban heat.

However, in the context of Melbourne, there is no snow and a growing interest in Water Sensitive Urban Design (WSUD) (Dahlenburg and Birtles, 2012). WSUD seeks to reduce runoff and increase infiltration in urban areas (Broadbent et al., 2018). For example, both urban greening and biofiltration systems reduce urban runoff, therefore mitigating downstream stream pollution and erosion (Hatt et al., 2004; Walsh et al., 2012), while also mitigating urban heat (Demuzere et al., 2014). For example, street trees in Melbourne were found to induce reductions of up to 1 °C in air temperature and 12 °C in UTCI (Coutts et al., 2015). This marked improvement in UTCI is predominately due to shading, which pavement watering cannot provide. Therefore, these techniques are more suited to mitigate urban heat in the Australian context.

However, these long-term solutions tend to require more planning and resources, and thus can take time to implement. Thus, although pavement watering is not an ideal long-term solution, it may be useful to provide immediate cooling in heat-related emergencies in Australia.

5. Conclusion

The viability of pavement watering as an urban heat mitigation technique was investigated with a series of carpark experiments. Pavement watering was found to reduce air temperature and improve thermal comfort in the right conditions, including low wind speeds and a high vapour-pressure deficit, with a maximum reduction of 0.6 °C and 2 °C for 1.5 m air temperature and the Universal Thermal Comfort Index respectively. A reduction of up to 9.0 °C in surface temperature was also found, and lower surface temperatures persisted even after the surface visibly dried. This resulted in reduced sensible heat flux during and after pavement watering. Thus, pavement watering has the potential to provide immediate cooling in Melbourne during times of extreme heat.

However, further research is needed to provide additional evidence for the benefits of pavement watering in Australia. This could include larger scale experiments with correctly calibrated sensors, with observations downwind of the watered area to understand the extent of cooling. Furthermore, it may be interesting to model the effect of pavement watering under a variety of background climate conditions, and thus be able to assess benefits in a controlled environment.

CRediT authorship contribution statement

Ellie Traill: Writing – original draft, Visualization, Methodology, Investigation, Formal analysis. **Kerry A. Nice:** Writing – review & editing, Supervision, Conceptualization. **Nigel Tapper:** Writing – review & editing, Supervision, Resources, Funding acquisition, Conceptualization. **Julie M. Arblaster:** Writing – review & editing, Supervision, Project administration.

Declaration of competing interest

None.

Data availability

Data will be made available on request.

Acknowledgements

KAN is supported by NHMRC/UKRI grant (1194959). ET and JMA acknowledge support from the Australian Research Council Centre of Excellence for Climate Extremes (170100023CE).

Appendix A. Daily weather observations

Table A1: The daily weather observations for Melbourne, Victoria for the experiment days in February 2022, taken from Bureau of Meteorology (2022).

Date	Min. T_a	Max. T_a	Daily Rain	9 am T_a	9 am RH	9 am Cld[a]	9 am Wind Dir.	9 am Wind	3 pm T_a	3 pm RH	3 pm Cld	3 pm Wind Dir.	3 pm Wind
	°C	°C	mm	°C	%	oktas		km/h	°C	%	oktas		km/h
7th	14.7	28.6	0	20.3	58	1	NE	7	27.2	40	1	S	13
8th	15.4	30.5	0	20	60	1	NNE	9	30	31	3	NE	6
12th	15.7	28.3	0	18.7	68	1	ESE	6	26.6	47	2	SSW	7
13th	17.1	32.1	0	23.5	50	4	NNW	20	30.3	34	7	NNW	20

[a] Fraction of sky obscured by cloud.

A.1. Sensor validation and corrections

As a result of the validation period for T_a and RH, T_a was discarded in favour of $T_{p,1.5}$ as both measured air temperature at 1.5 m, and there were clear issues with the control T_a sensor. The mean difference between RH control and experimental sensors from this validation period was calculated (2.5%) and used to correct the experiment data.

During the validation period for the Kestrels (K_T and K_{RH}), K_T was considered reasonable, while the mean difference between K_{RH} sensors from this validation period was calculated (3.8%) and applied to experiment data.

During the validation period for T_g, $K\downarrow$, $K\uparrow$, $L\downarrow$, and $L\uparrow$, the T_g, $K\downarrow$, and $K\uparrow$ was considered reasonable, while $L\downarrow$ and $L\uparrow$ were not comparable.

The CNR1 measures the exchange of thermal radiation between the sensor and the object being faced (L_{raw}), which is then used alongside the temperature of the CNR1 (T_{CNR1}) to calculate L as follows:

$$L = L_{raw} + \sigma(T_{CNR1} + 273.15)^4 \quad (A.1)$$

where σ is the Stefan-Boltzmann constant ($5.67 \times 10^{-8} Wm^{-2}K^{-4}$) (Campbell Campbell Scientific, 2011).

Type E thermocouples were attached to the bottom of the CNR1 sensors to measure its temperature ($T_{CNR1,ext}$) instead of the CNR1 internal temperature sensors ($T_{CNR1,int}$) due to limited inputs on the data loggers. It can be seen that the $T_{CNR1,ext}$, not the $L{\downarrow}_{raw}$, $L{\uparrow}_{raw}$ was causing the difference between control and experimental L.

Additional investigation found that the internal temperature of the control and experimental CNR1 do not vary significantly, and thus it is likely that one or both of the thermocouples were not placed appropriately and/or securely on the CNR1. Therefore, the assumption was made that the actual T_{CNR1} did not vary between the control and experimental sensors. Thus, $L\downarrow$ and $L\uparrow$ was corrected with calculations based on the same CNR1 temperature.

The control $T_{CNR1,ext}$ was identified as the 'correct' temperature was based on deriving the surface temperature ($T_{s,drvd}$) (see Appendix A.3.2).

A.2. Derived variables

A.2.1. Wind speed 10 m

It should be noted that the wind profile of the atmospheric boundary layer is generally logarithmic, and thus is commonly approximated using the log wind profile equation (Bañuelos-Ruedas et al., 2010). However, this requires the surface roughness and atmospheric stability to be known. Thus, to avoid assumptions and uncertainties associated with these variables, and as wind was measured at two heights, the wind profile power law (also known as the Hellmann exponential law) was used. This is commonly used when information is limited, although it is less theoretically accurate (Bañuelos-Ruedas et al., 2010).

The wind profile power law is defined as:

$$u_2 = u_1 \left(\frac{z_2}{z_1}\right)^{\alpha} \quad (A.2)$$

where u_1 and u_2 is wind speed (ms^{-1}) at height z_1 and z_2(m) respectively, and α is the wind shear exponent (Manwell et al., 2010). Firstly, α was derived from measured wind speed at 0.3 m (K_u) and 2.25 m (u). The average of the control and experimental K_u values was used as it is assumed that the wind speed was the same for the control and experimental sites, as they were within 10 m of each other. The average α was then used to calculate wind speed at 10 m (u_{10}).

A.2.2. Surface temperature

Only the experimental station had a surface temperature sensor (T_s) (Fig. 1), thus surface temperature was derived for the control and experimental station ($T_{s,drvd}$), the latter for verification and consistency. $L\uparrow(Wm^{-2})$ and T_s(°C) are related to each other by the following equation:

$$L\uparrow = \epsilon\sigma(T_s + 273.15)^4 + (1-\epsilon)L\downarrow \quad (A.3)$$

where σ is the Stefan-Boltzmann constant ($5.67 \times 10^{-8} Wm^{-2}K^{-4}$) and ϵ is emissivity of the surface (−). The magnitude of ϵ is unknown, but for road surfaces is commonly above 0.85 (Oke et al., 2017). Assuming that the surface is a black body (i.e., $\epsilon = 1$) and rewriting to solve for $T_{s,drvd}$ simplifies the equation to:

$$T_{s,drvd} = \left(\frac{L\uparrow}{\sigma}\right)^{0.25} - 273.15 \quad (A.4)$$

As $L\uparrow$ was found to impacted by errors associated with T_{CNR1} (Appendix A.2), $L\uparrow$ was calculated using both the control and experimental T_{CNR1} (Eq. A.1) before being used to calculate $T_{s,drvd}$ (Eq. A.4). Comparing the experimental $T_{s,drvd}$ with measured T_s showed that the black body assumption is flawed (Fig. A.8). To overcome this, the terms ignored in Eq. A.4 were indirectly accounted for by performing a linear regression between T_s and $T_{s,drvd}$ and applying this calculated linear model for each experiment day.

The results of the different methods to calculate experimental $T_{s,drvd}$ alongside measured T_s are shown in Fig. A.8. It is clear that the $T_{s,drvd}$ computed with linear model using the $L\uparrow$ calculated with the control T_{CNR1} replicates the measured T_s well. This is also shown as this method had the best performing R^2 values, which were 0.98, 0.98, and 0.96 for the 8th, 12th, and 13th respectively. This implies that the control T_{CNR1} captured the 'correct' temperature of the CNR1 sensor, while the experimental T_{CNR1} sensor may have been in an incorrect position.

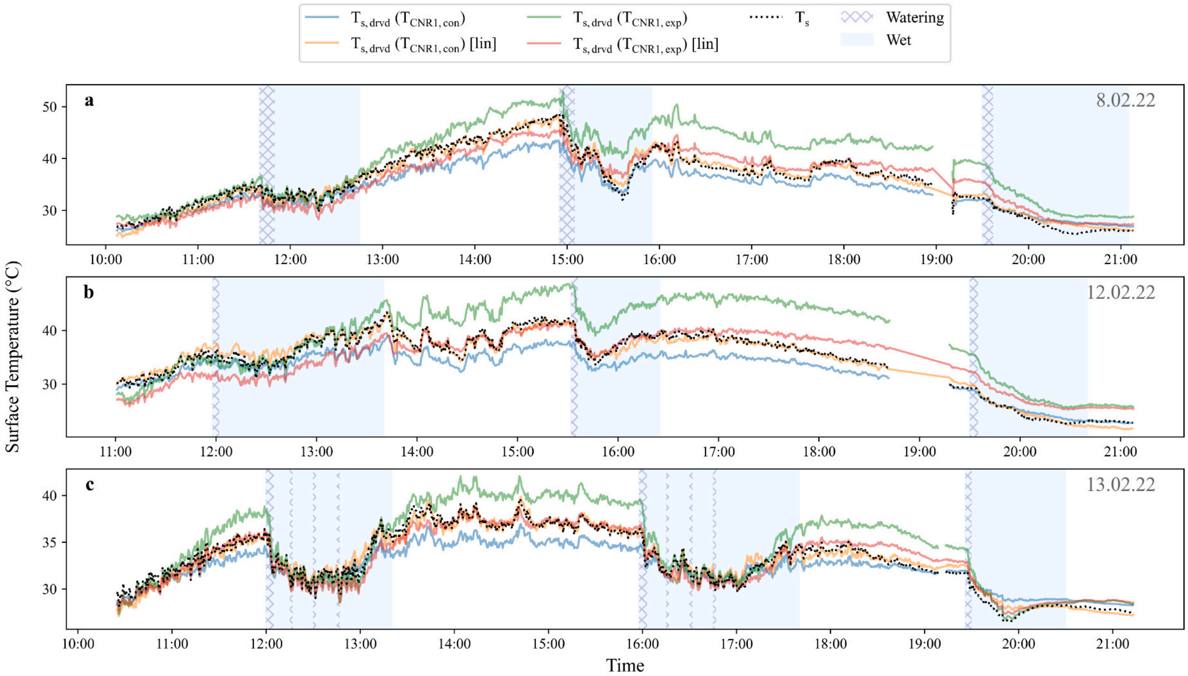

Fig. A.8: Different methods to derive surface temperature ($T_{s,drvd}$) for the experimental site compared to measured (T_s) for the experiment days: (a) 8th, (b) 12th, (c) 13th.

$T_{s,drvd}$ was then calculated for the control station using the calculated linear model along with $L\uparrow$ calculated with the control T_{CNR1} (Fig. A.17 and Table A3). For consistency, $T_{s,drvd}$ was used for both the control and experimental surface temperature to interpret impacts of watering, rather than T_s.

A.2.3. Vapour-pressure deficit

Instead of *RH*, a more accurate way to express the driving force of water loss is vapour- pressure deficit (VPD). VPD (kPa) is defined as the difference between the saturated vapour pressure (e_s, kPa) and the ambient vapour pressure (e_a, kPa). The e_s can be calculated as:

$$e_s = ae^{\left(\frac{bT_{p,1.5}}{T_{p,1.5}+c}\right)} \tag{A.5}$$

where a, b, and c are constants. As suggested by McMahon et al. (2013), constants defined by Allen et al. (1998) are used (a = 0.6108 kPa, b = 17.27, c = 237.3 °C). Relative humidity (*RH*,%) is the vapour pressure ratio, and thus VPD can be written as:

$$VPD = e_s\left(1 - \frac{RH}{100}\right) \tag{A.6}$$

$T_{p,1.5}$ and *RH* from the control and experimental stations (Fig. 1) were used to calculate VPD. As the $T_{p,1.5}$ was not working for the majority of experiment 13 M, VPD could not be calculated for this experiment, however, it can be assumed it was quite high given the other VPD values on the 13th.

A.2.4. Mean radiant temperature and the universal thermal climate index

To calculate the mean radiant temperature (T_{MRT}, K), the pythermalcomfort python package was used (Tartarini and Schiavon, 2020). This employs the formula specified by ISO 7726:1998 Standard. Firstly, the heat transfer coefficient (*h*) is calculated as the maximum value between natural and forced convection as follows:

$$h = max\begin{cases} \dfrac{1.4\cdot|tg - tbd|^{0.25}}{d} \\ 6.3\dfrac{v^{0.6}}{d^{0.4}} \end{cases} \tag{A.7}$$

where *tg* is global temperature (K), *tdb* is air temperature (K), *v* is the wind speed (ms^{-1}), and *d* is the diameter of the globe (m). T_{MRT} can then be calculated as follows:

$$T_{MRT} = \left(tg^4 + h\frac{tg - tbd}{\epsilon \cdot 5.67 \times 10^{-8}} \right)^{0.25} \tag{A.8}$$

where ϵ is the emissivity of the globe.

The library pythermalcomfort facilitated the conversion of units, thus T_g, $T_{p,1.5}$, and u were used to calculate T_{MRT}. For the globe diameter and emissivity, Campbell Scientific BlackGlobe values of 0.152 m and 0.957 respectively were used (Campbell Scientific, 2022). T_{MRT} was also converted to °C.

The same python library was used to calculate the Universal Thermal Climate Index (UTCI,°C), a mathematical model that assesses the outdoor thermal environment and provides an indicator for heat stress. The model requires $T_{p,1.5}$, T_{MRT}, u_{10} (ms^{-1}), and RH (%).

A.2.5. Surface energy balance

Latent heat flux (Q_E, Wm^{-2}) was calculated as:

$$Q_e = \ell_v \rho_w \frac{V}{A}\frac{1}{t}\frac{1m}{1000mm} \tag{A.9}$$

where ℓ_v is the latent heat of vaporisation (2.5×10^6 J kg^{-1}), ρ_w is the density of water (1000 kg m^{-3}), V is the volume of water (L), A is the area watered (10 m × 10 m), t is the total time to evaporate (seconds), and the last term converts the units to Wm^{-2}. The t was taken as the time it took for the area under the experimental station to become dry after watering.

The V was adjusted to take into account water accumulation on the edge of the watered plot and losses due to runoff, based on observations. The carpark was slightly sloped towards the edges, and despite efforts to contain water inside the established plot, there was significant build up along the west edge and varying amounts of runoff (Fig. 1, Table 3). It was assumed that there was no drainage, as the surface did not appear to have any cracks and any infiltration was considered negligible. It was also assumed that the water storage capacity of the plot was 40 L when subtracted for runoff and edge build up, and thus V = 40 L was used to calculate Q_E. For the experiments where 20 L was added after the initial watering at set intervals (13 M and 13 A), as this water was added to the east side of the plot and resulted in no observable extra runoff or build-up, 40 L from the initial 60 L was added to the following 20 L (i.e., $V =$ 100 L).

To calculate sensible heat flux (Q_H, Wm^{-2}), the following formula was used:

$$Q_H = \rho_a C_p \frac{(T_s - T_a)}{r_{ah}} \tag{A.10}$$

where ρ_a is the density of air (1.2041 kg m^{-3}), C_p is the specific heat of air at constant pressure (1.005×10^3 kg m^{-3}), T_s is the surface temperature (°C), T_a is the air temperature (°C), and r_{ah} is the aerodynamic resistance to heat transfer. r_{ah} was calculated using an equation derived from the Monin-Obukhov Similarity Theory, where assuming neutral conditions, it can be written as:

$$r_{ah} = \frac{1}{k^2 u}\left[ln\left(\frac{Z-d}{z_{0m}}\right)\right]\left[ln\left(\frac{Z-d}{z_{0h}}\right)\right] \tag{A.11}$$

where k is the von Karman constant (0.41), u is the wind speed (ms^{-1}) at reference height Z (m), and d is the zero-plane displacement (Liu et al., 2007).

The roughness length for momentum transfer (z_{0m}) and the roughness length for heat transfer (z_{0h}) were set as 0.09 and $e^{-9.4}$ respectively, based on results from an outdoor urban scale model made of concrete cubes (Kanda et al., 2007). $T_{s,drvd}$, $T_{p,0.05}$, and u_{10} was used for the surface temperature, air temperature, and wind respectively. Air temperature at the lowest height (0.05 m) was chosen as it plausibly has the most interaction with surface temperature, and thus the most relevance for Q_H.

Appendix B. Supplementary data

Supplementary data to this article can be found online at https://doi.org/10.1016/j.uclim.2024.102042.

References

ABS, 2013. 3222.0 - population projections, Australia, 2012 (base) to 2101. Australian Bureau of Statistics. http://www.abs.gov.au/Ausstats/abs@.nsf/mf/3222.0.

Allen, R.G., Pereira, L.S., Raes, D., Smith, M., 1998. Crop Evapotranspiration-Guidelines for Computing Crop Water Requirements, 300. FAO. D05109.

Anandakumar, K., 1999. A study on the partition of net radiation into heat fluxes on a dry asphalt surface. Atmos. Environ. 33, 3911–3918.

Bañuelos-Ruedas, F., Angeles-Camacho, C., Rios-Marcuello, S., 2010. Analysis and validation of the methodology used in the extrapolation of wind speed data at different heights. Renew. Sust. Energ. Rev. 14, 2383–2391. https://doi.org/10.1016/j.rser.2010.05.001.

Beck, H.E., Zimmermann, N.E., McVicar, T.R., Vergopolan, N., Berg, A., Wood, E.F., 2018. Present and future Köppen-Geiger climate classification maps at 1-km resolution. Scientific Data 5, 180214. https://doi.org/10.1038/sdata.2018.214.

Broadbent, A.M., Coutts, A.M., Tapper, N.J., Demuzere, M., 2018. The cooling effect of irrigation on urban microclimate during heatwave conditions. Urban Clim. 23, 309–329. https://doi.org/10.1016/j.uclim.2017.05.002.

Brunner, J., Cozens, P., 2013. 'Where have all the trees gone?' Urban consolidation and the demise of urban vegetation: a case study from Western Australia. Plan. Pract. Res. 28, 231–255. https://doi.org/10.1080/02697459.2012.733525.

Bureau of Meteorology, 2022. Melbourne (Olympic Park). Daily Weather Observations, Victoria. http://www.bom.gov.au/climate/dwo/202202/html/IDCJDW3050.202202.shtml.
Campbell Scientific, 2011. CNR1 Net Radiometer Instruction Manual. URL. https://s.campbellsci.com/documents/au/manuals/cnr1.pdf.
Campbell Scientific, 2022. BlackGlobe Temperature Sensor for Heat Stress Product Manual. URL. https://s.campbellsci.com/documents/au/manuals/blackglobe.pdf.
Cheung, P.K., Jim, C.Y., Tapper, N., Nice, K.A., Livesley, S.J., 2022. Daytime irrigation leads to significantly cooler private backyards in summer. Urban Clim. 46, 101310 https://doi.org/10.1016/j.uclim.2022.101310.
Clarke, J.F., 1972. Some effects of the urban structure on heat mortality. Environ. Res. 5, 93–104. https://doi.org/10.1016/0013-9351(72)90023-0.
Coates, L., Haynes, K., O'Brien, J., et al., 2014. Exploring 167 years of vulnerability: an examination of extreme heat events in Australia 1844-2010. Environ. Sci. Pol. 42, 33–44. https://doi.org/10.1016/j.envsci.2014.05.003.
Cohard, J.M., Rosant, J.M., Rodriguez, F., Andrieu, H., Mestayer, P.G., Guillevic, P., 2018. Energy and water budgets of asphalt concrete pavement under simulated rain events. Urban Clim. 24, 675–691. https://doi.org/10.1016/j.uclim.2017.08.009.
Coutts, A.M., Beringer, J., Tapper, N., 2010. Changing urban climate and CO2 emissions: implications for the development of policies for sustainable cities. Urban Policy Res. 28, 27–47. https://doi.org/10.1080/08111140903437716.
Coutts, A.M., Tapper, N.J., Beringer, J., Loughnan, M., Demuzere, M., 2012. Watering our cities: the capacity for water sensitive Urban Design to support urban cooling and improve human thermal comfort in the Australian context. Prog. Phys. Geogr. 37, 2–28. https://doi.org/10.1177/0309133312461032.
Coutts, A.M., White, E.C., Tapper, N.J., Beringer, J., Livesley, S.J., 2015. Temperature and human thermal comfort effects of street trees across three contrasting street canyon environments. Theor. Appl. Climatol. 124, 55–68. https://doi.org/10.1007/s00704-015-1409-y.
Cowan, T., Purich, A., Perkins, S., Pezza, A., Boschat, G., Sadler, K., 2014. More frequent, longer, and hotter heat waves for Australia in the twenty-first century. J. Clim. 27, 5851–5871. https://doi.org/10.1175/JCLI-D-14-00092.1.
Dahlenburg, J., Birtles, P., 2012. All roads lead to WSUD: Exploring the biodiversity, human health and social benefits of WSUD. In: 7th International Conference on Water Sensitive Urban Design, February 2012 Melbourne, Australia.
Daniel, M., Lemonsu, A., Viguié, V., 2018. Role of watering practices in large-scale urban planning strategies to face the heat-wave risk in future climate. Urban Clim. 23, 287–308. https://doi.org/10.1016/j.uclim.2016.11.001.
Demuzere, M., Coutts, A.M., Göhler, M., Broadbent, A.M., Wouters, H., van Lipzig, N.P.M., Gebert, L., 2014. The implementation of biofiltration systems, rainwater tanks and urban irrigation in a single-layer urban canopy model. Urban Clim. 10, 148–170. https://doi.org/10.1016/j.uclim.2014.10.012.
Forzieri, G., Cescatti, A., Batista, F., Feyen, L., 2017. Increasing risk over time of weather-related hazards to the European population: a data-driven prognostic study. Lancet Planet Health 1, e200–e208. https://doi.org/10.1016/S2542-5196(17)30082-7.
Hatt, B.E., Fletcher, T.D., Walsh, C.J., Taylor, S.L., 2004. The influence of urban density and drainage infrastructure on the concentrations and loads of pollutants in small streams. Environ. Manag. 34, 112–124. https://doi.org/10.1007/s00267-004-0221-8.
Heidari, H., Mohammadbeigi, A., Khazaei, S., Soltanzadeha, A., Asgariand, A., Saghafipoure, A., 2020. The effects of climatic and environmental factors on heat-related illnesses: a systematic review from 2000 to 2020. Urban Clim. 34, 100720 https://doi.org/10.1016/j.uclim.2020.100720.
Hendel, M., Royon, L., 2015. The effect of pavement-watering on subsurface pavement temperatures. Urban Clim. 14, 650–654. https://doi.org/10.1016/j.uclim.2015.10.006.
Hendel, M., Colombert, M., Diab, Y., Royon, L., 2014. Improving a pavement-watering method on the basis of pavement surface temperature measurements. Urban Clim. 189–200 https://doi.org/10.1016/j.uclim.2014.11.002.
Hendel, M., Colombert, M., Diab, Y., Royon, L., 2015a. An analysis of pavement heat flux to optimize the water efficiency of a pavement-watering method. Appl. Therm. Eng. 78, 658–669. https://doi.org/10.1016/j.applthermaleng.2014.11.060.
Hendel, M., Gutierrez, P., Colombert, M., Diab, Y., Royon, L., 2016. Measuring the effects of urban heat island mitigation techniques in the field: application to the case of pavement-watering in Paris. Urban Clim. 16, 43–58. https://doi.org/10.1016/j.uclim.2016.02.003.
Hendel, M., Bobée, C., Karam, G., Parison, S., Berthe, A., Bordin, P., 2020. Developing a GIS tool for emergency urban cooling in case of heat-waves. Urban Clim. 33, 100646 https://doi.org/10.1016/j.uclim.2020.100646.
Hendel, M.A., Colombert, M., Diab, Y., Royon, L., 2015b. Measurement of the cooling efficiency of pavement-watering as an urban Heat Island mitigation technique. J. Sustain. Develop. Energy, Water Environ. Syst. 3, 1–11.
Himeno, S., Takahashi, R., Asakura, A., Koike, K., Fujita, S., 2010. Using snow melting pipes to verify the water sprinkling s effect over a wide area. In: Novatech 2010, 7th International Conference on Sustainable Techniques and Strategies for Urban Water Management, Jun 2010, Lyon, France. URL. https://hal.archives-ouvertes.fr/hal-03295968.
IPCC, 2022. Climate change 2022: Impacts, adaptation, and vulnerability. In: Contribution of Working Group II to the Sixth Assessment Report of the Intergovernmental Panel on Climate Change. Cambridge University Press.
Kanda, M., Kanega, M., Kawai, T., Moriwaki, R., Sugawara, H., 2007. Roughness lengths for momentum and heat derived from outdoor urban scale models. J. Appl. Meteorol. Climatol. 46, 1067–1079. https://doi.org/10.1175/JAM2500.1.
Kim, S.R., Jung, E.H., Kim, H.D., 2014. Evaluation on the effect of air quality improvement due to the employment of clean-road system in Daegu. J. Environ. Sci. Intern. 23, 2029–2034. https://doi.org/10.5322/JESI.2014.23.12.2029.
Kim, S.R., Jung, E.H., Kim, H.D., 2015. Observational study to investigate thermal environment and effect of clean-road system over a broad way of Daegu in summer. J. Environ. Sci. Intern. 24, 1171–1180. https://doi.org/10.5322/JESI.2015.24.9.1171.
Kinouchi, T., 1997. An observation on the climatic effect of watering on paved roads. J. Hydrosci. Hydraul. Eng. 14, 55–64.
Krayenhoff, E.S., Broadbent, A.M., Zhao, L., Georgescu, M., Middel, A., Voogt, J.A., Martilli, A., Sailor, D.J., Erell, E., 2021. Cooling hot cities: a systematic and critical review of the numerical modelling literature. Environ. Res. Lett. 16, 053007. https://doi.org/10.1088/1748-9326/abdcf1.
Kubilay, A., Ferrari, A., Derome, D., Carmeliet, J., 2021. Smart wetting of permeable pavements as measure for improving the urban climate during heat waves. J. Build. Phys. 45, 36–66. https://doi.org/10.1177/1744259120968586.
Liu, S., Lu, L., Mao, D., Jia, L., 2007. Evaluating parameterizations of aerodynamic resistance to heat transfer using field measurements. Hydrol. Earth Syst. Sci. 11, 769–783. https://doi.org/10.5194/hess-11-769-2007.
Liu, Y., Ma, H., Zhang, C., Luo, X., 2022. Watering on porous pavement for improvement of environmental human thermal comfort in an ecological community in arid area: a case study in Lanzhou, China. Sustain. Cities Soc. 85, 104081 https://doi.org/10.1016/j.scs.2022.104081.
Loughnan, M.E., Nicholls, N., Tapper, N.J., 2010. When the heat is on: threshold temperatures for AMI admissions to hospital in Melbourne Australia. Appl. Geogr. 30, 63–69. https://doi.org/10.1016/j.apgeog.2009.08.003.
Manwell, J.F., McGowan, J.G., Rogers, A.L., 2010. Wind Energy Explained: Theory, Design and Application. John Wiley & Sons.
Martilli, A., Krayenhoff, E.S., Nazarian, N., 2020. Is the urban Heat Island intensity relevant for heat mitigation studies? Urban Clim. 31 https://doi.org/10.1016/j.uclim.2019.100541.
McMahon, T.A., Peel, M.C., Lowe, L., Srikanthan, R., McVicar, T.R., 2013. Estimating actual, potential, reference crop and pan evaporation using standard meteorological data: a pragmatic synthesis. Hydrol. Earth Syst. Sci. 17, 1331–1363. https://doi.org/10.5194/hess-17-1331-2013.
Middel, A., Krayenhoff, E.S., 2019. Micrometeorological determinants of pedestrian thermal exposure during record-breaking heat in Tempe, Arizona: introducing the MaRTy observational platform. Sci. Total Environ. 687, 137–151. https://doi.org/10.1016/j.scitotenv.2019.06.085.
Middel, A., AlKhaled, S., Schneider, F.A., Hagen, B., Coseo, P., 2021. 50 Grades of Shade. BAMS. https://doi.org/10.1175/BAMS-D-20-0193.1.
Motazedian, A., Coutts, A.M., Tapper, N.J., 2020. The microclimatic interaction of a small urban park in Central Melbourne with its surrounding urban environment during heat events. Urban For. Urban Green. https://doi.org/10.1016/j.ufug.2020.126688.
Na, M.S., Shin, D.U., Kim, Y.G., 2021. Study on the effect of timestep and thermography method for pavement watering technology. Urban Clim. 39, 100920 https://doi.org/10.1016/j.uclim.2021.100920.

Nazarian, N., Krayenhoff, E.S., Bechtel, B., Hondula, D.M., Paolini, R., Vanos, J., Cheung, T., Chow, W.T.L., de Dear, R., Jay, O., Lee, J.K.W., Martilli, A., Middel, A., Norford, L.K., Sadeghi, M., Schiavon, S., Santamouris, M., 2022. Integrated assessment of urban overheating impacts on human life earth's future. Earth's Future 10. https://doi.org/10.1029/2022EF002682 e2022EF002682.
Nearmap, 2022. Nearmap Aerial Imagery.
Nice, K.A., Nazarian, N., Lipson, M.J., Hart, M.A., Seneviratne, S., Thompson, J., Naserikia, M., Godic, B., Stevenson, M., 2022. Isolating the impacts of urban form and fabric from geography on urban heat and human thermal comfort. Build. Environ. https://doi.org/10.1016/j.buildenv.2022.109502.
Nicholls, N., Skinner, C., Loughnan, M., et al., 2008. A simple heat alert system for Melbourne, Australia. Int. J. Biometeorol. 52, 375–384. https://doi.org/10.1007/s00484-007-0132-5.
Oke, T., 1982. The energetic basis of the urban heat island. Q. J. R. Meteorol. Soc. 108, 1–24. https://doi.org/10.1002/qj.49710845502/abstract.
Oke, T.R., 1989. The micrometeorology of the urban forest. Philos. Transact. Roy. Soc. Lond. Ser. B, Biol. Sci. 324, 335–349. http://rstb.royalsocietypublishing.org/content/324/1223/335.short.
Oke, T.R., Mills, G., Christen, A., Voogt, J.A., 2017. Urban Climates. Cambridge University Press, Cambridge. https://doi.org/10.1017/9781139016476.
Parison, S., Hendel, M., Royon, L., 2020. A statistical method for quantifying the field effects of urban heat island mitigation techniques. Urban Clim. 33, 100651 https://doi.org/10.1016/j.uclim.2020.100651.
Pascal, M., Laaidi, K., Ledrans, M., Baffert, E., Caserio-Schönemann, C., Tertre, A.L., Manach, J., Medina, S., Rudant, J., Empereur-Bissonnet, P., 2006. France's heat health watch warning system. Int. J. Biometeorol. 50, 144–153. https://doi.org/10.1007/s00484-005-0003-x.
Pasquill, F., 1961. The estimation of the dispersion of windborne material. Meteorol. Mag. 90, 33–49.
Perkins-Kirkpatrick, S.E., Lewis, S.C., 2020. Increasing trends in regional heatwaves. Nat. Commun. 11 https://doi.org/10.1038/s41467-020-16970-7.
Phillips, S.D., Estler, W.T., Doiron, T., Eberhardt, K.R., Levenson, M.S., 2001. A careful consideration of the calibration concept. J. Res. Natl. Inst. Stand. Technol. 106, 371–379. https://doi.org/10.6028/jres.106.014.
Sandia National Laboratories, 2024. Albedo - PV Performance Modeling Collaborative (PVPMC). https://pvpmc.sandia.gov/modeling-guide/1-weather-design-inputs/plane-of-array-poa-irradiance/calculating-poa-irradiance/poa-ground-reflected/albedo/ (Accessed 14 May 2024).
Solcerova, A., van Emmerik, T., Hilgersom, K., van de Ven, F., van de Giesen, N., 2018. Uchimizu: a cool(ing) tradition to locally decrease air temperature. Water 10. https://doi.org/10.3390/w10060741.
Spronken-Smith, R.A., Oke, T.R., 2010. The thermal regime of urban parks in two cities with different summer climates. Int. J. Remote Sens. 19, 2085–2104. https://doi.org/10.1080/014311698214884.
Takebayashi, H., Danno, H., Tozawa, U., 2021. Study on appropriate heat mitigation technologies for urban block redevelopment based on demonstration experiments in Kobe city. Energy Build. 250, 111299 https://doi.org/10.1016/j.enbuild.2021.111299.
Takebayashi, H., Danno, H., Tozawa, U., 2022. Study on strategies to implement adaptation measures for extreme high temperatures into the street canyon. Atmosphere 13, 946. https://doi.org/10.3390/atmos13060946.
Takebayashi, H., Mori, H., Tozawa, U., 2023. Study on an effective roadway watering scheme for mitigating pedestrian thermal comfort according to the street configuration. Atmosphere 14, 1014. https://doi.org/10.3390/atmos14061014.
Tartarini, F., Schiavon, S., 2020. Pythermalcomfort: a Python package for thermal comfort research. SoftwareX 12, 100578. https://doi.org/10.1016/j.softx.2020.100578.
Walsh, C.J., Fletcher, T.D., Burns, M.J., 2012. Urban Stormwater runoff: a new class of environmental flow problem. PLoS One 7, e45814. https://doi.org/10.1371/journal.pone.0045814.
Wang, J., Meng, Q., Tan, K., Santamouris, M., 2022. Evaporative cooling performance estimation of pervious pavement based on evaporation resistance. Build. Environ. 217, 109083 https://doi.org/10.1016/j.buildenv.2022.109083.
Wilson, L., 2011. Heatwaves and the elderly: the role of the GP in reducing morbidity. Aust. Fam. Physician 40, 637–640.
Zare, S., Hasheminejad, N., Elahi, H., Hemmatjo, R., Sarebanzadeh, K., Ahmadi, S., 2018. Comparing universal thermal climate index (UTCI) with selected thermal indices/environmental parameters during 12 months of the year. Weather and climate. Extremes 19, 49–57. https://doi.org/10.1016/j.wace.2018.01.004.